Research Square

Preprints are preliminary reports that have not undergone peer review.
They should not be considered conclusive, used to inform clinical practice,
or referenced by the media as validated information.

Non-invasive Prediction of Molecular and Histopathological Subtypes in Murine and Human Pancreatic Ductal Adenocarcinoma Using [^{18}F]FDG PET

Romina Karampour

romina.karampour@tum.de

Department of Diagnostic and Interventional Radiology, Technical University of Munich, School of Medicine and Health, TUM University Hospital rechts der Isar https://orcid.org/0000-0002-5649-0761

Irina Heid

irina.heid@tum.de

Department of Diagnostic and Interventional Radiology, Technical University of Munich, School of Medicine and Health, TUM University Hospital, Klinikum Rechts der Isar, Munich, Germany.
https://orcid.org/0000-0002-9834-2820

Research Article

Keywords: Pancreatic ductal adenocarcinoma (PDAC), [18F]FDG PET, classical/quasi-mesenchymal, gland-forming/non-gland-forming, QM/non-QM

Posted Date: November 19th, 2026

DOI: https://doi.org/10.21203/rs.3.rs-11729028/v1

License: This work is licensed under a Creative Commons Attribution 4.0 International License.
Read Full License

Additional Declarations: The authors declare no competing interests.

Abstract

Purpose

This study evaluates the utility of [^{18}F]fluorodeoxyglucose positron emission tomography ([^{18}F]FDG PET) for Pancreatic ductal adenocarcinoma (PDAC) subtype differentiation across preclinical and clinical settings, and assesses the impact of tracer uptake timing on subtype discrimination.

Methods

[^{18}F]FDG uptake was investigated in classical (C)-HPAC and quasi-mesenchymal (QM)-PSN1 cells, heterotopic rat (n = 11), orthotopic mouse xenografts (n = 8), and gland-forming (GF)/non-GF tumors from seven genetically engineered mouse models (GEMMs). Retrospective [^{18}F]FDG PET data from 16 PDAC patients were analyzed using subtype classification based on keratin-81 (KRT81+(QM)/KRT81-(non-QM)). Dynamic and static [^{18}F]FDG PET parameters, including standard uptake value $(SUV)_{mean}$, SUV_{max}, and mean tumor-to-muscle ratio (T/M_{mean}), were evaluated for subtype discrimination.

Results

QM tumors showed significantly higher [^{18}F]FDG uptake than C tumors *in vitro* (50.7 ± 1.03% vs. 19.4 ± 2.37%), in heterotopic (SUV_{max} 6.91 ± 1.14 vs. 2.66 ± 0.28), and orthotopic (SUV_{max} 2.85 ± 0.70 vs. 1.45 ± 0.50) xenografts. Non-GF tumors also showed significantly higher uptake than GF (SUV_{max} 3.94 ± 0.70 vs. 2.53 ± 0.97). Patients showed a similar trend (SUV_{max} 6.33 ± 1.74 vs. 4.95 ± 1.46), with shorter overall survival in QM tumors. Dynamic PET revealed continued tracer accumulation in QM/non-GF tumors throughout the 90-minute acquisition period, whereas C/GF tumors approached a plateau by approximately 60 minutes. T/M_{mean} showed the best classification performance across all models.

Conclusion

[^{18}F]FDG PET differentiated PDAC subtypes across all preclinical models with a similar but less pronounced trend in patients. Later imaging time points showed enhanced metabolic separation, suggesting potential benefits for improving non-invasive subtype discrimination.

Clinical Trial Registration

N/A

Introduction

Pancreatic cancer remains highly lethal, with a 5-year survival rate of approximately 13% [1], and its incidence is projected to rise substantially in the coming decades[2]. Pancreatic ductal adenocarcinoma (PDAC), the most common type of pancreatic cancer, is marked by substantial inter- and intratumoral molecular and histological heterogeneity[3], which drives variable tumor behavior and treatment response, highlighting the need for patient stratification.

Molecular profiling has identified distinct PDAC subtypes: classical (C), characterized by high expression of epithelial and adhesion-associated genes; quasi-mesenchymal (QM), marked by increased mesenchyme-associated gene expression; and exocrine-like, characterized by increased digestive enzyme gene expression[4–6]. Related classification systems broadly align pancreatic progenitors and basal-like/squamous phenotypes with C and QM tumors, respectively [4, 7, 8]. Histomorphologic classification into gland-forming (GF) and non–gland-forming (non-GF) patterns correlated with established molecular subtypes and predicted clinical outcome better than differentiation-based stratification [9].

PDAC subtypes respond differently to systemic therapies. Basal-like tumors showed a trend toward improved survival with gemcitabine/nab-paclitaxel [10], whereas C tumors showed longer progression-free and overall survival with FOLFIRINOX (folinic acid, fluorouracil, irinotecan, and oxaliplatin) [11], highlighting the need for accurate subtyping before treatment selection. Molecular subtyping, however, requires tumor tissue and specialized profiling, which is invasive, high-cost, expert-dependent, and data-intensive, limiting its routine clinical implementation and longitudinal assessment of tumor phenotype [12]. Radiomics offers a noninvasive alternative, using computed tomography (CT)- and magnetic resonance imaging (MRI)-based machine learning models to predict QM/non-QM PDAC subtypes from imaging data [13, 14]. Yet these approaches rely on extracting and analyzing large numbers of imaging features, raising the question of whether simpler, readily available quantitative imaging parameters can provide complementary information on PDAC phenotype.

^{18}F-fluorodeoxyglucose positron emission tomography ([^{18}F]FDG PET) enables non-invasive visualization and quantification of tumor glucose uptake[15, 16]. In pancreatic cancer, it detects primary pancreatic carcinomas with a pooled sensitivity of 91% and specificity of 81% across 30 studies involving 1582 patients[17]. Higher [^{18}F]FDG PET uptake has been associated with more aggressive tumors and poorer clinical outcomes[18–20]. Also, early changes in [^{18}F]FDG PET metabolic parameters, as early as 2 weeks after treatment initiation, have shown potential to predict chemotherapy response in PDAC [21].

Oncogenic KRAS, the most frequent genetic alteration in PDAC [22], upregulates glucose transporter 1 (GLUT1) and glycolytic enzymes like hexokinases (HK) [23, 24]. Increased KRAS dosage was also linked to poorly differentiated tumors, advanced metastatic disease, and poorer survival in PDAC [25–27]. Consistently, poorly differentiated tumors showed higher [^{18}F]FDG uptake than well-differentiated tumors[28]. Integrating metabolic and molecular imaging with existing molecular and pathological frameworks is a critical step toward precision oncology in PDAC.

Despite this biological rationale, it remains unclear whether conventional [^{18}F]FDG PET parameters can differentiate PDAC phenotypes and whether subtype-associated differences depend on tracer uptake time. We therefore investigated the metabolic features of molecular and histomorphological PDAC subtypes using [^{18}F]FDG PET imaging across *in vitro*, heterotopic, orthotopic, genetically engineered mouse models (GEMMs), and a retrospective patient cohort. We further investigated whether reference-tissue normalization influences metabolic differentiation of PDAC phenotypes.

Materials and methods

Cell culture and cell preparation for implantation:

Human PDAC cell lines QM-PSN1(RRID: CVCL_1644) and C-HPAC (RRID: CVCL_3517) were obtained from ATCC and externally verified. Further procedures are described in supplementary methods (Online Resource 1).

In vitro [^{18}F]FDG uptake assay:

Cells were seeded in 12-well plates (170,000 cells/well) 48 h before the experiment. For glucose starvation, medium was replaced with glucose-free RPMI 2 h before adding 0.25MBq [^{18}F]FDG/well. Uptake was measured at 0, 15, 30, 60, and 90 min using a 2480 WIZARD automatic gamma counter (PerkinElmer, USA) and expressed as the percentage of cellular radioactivity relative to total measured radioactivity. Detailed procedures are provided in the supplementary methods (Online Resource 1).

Tumor models:

All animal experiments were approved by the Regierung von Oberbayern (Munich, Germany; license 55.2–2532.Vet_02-18-91), performed in compliance with the European guidelines for the care and use of laboratory animals, and reported in accordance with the ARRIVE guidelines. Euthanasia was performed by cervical dislocation under deep isoflurane anesthesia.

For heterotopic xenografts, *Crl:NIH*-Foxn1^{rnu} rats received subcutaneous injections of 10^7 QM-PSN1 (n = 5) or C-HPAC (n = 6) cells [29–31]. For orthotopic xenografts, 5,000 QM-PSN1 (n = 3) or C-HPAC (n = 5) cells were implanted into the pancreas of *CRL:NU(NCr)*-Foxn1^{nu} mice [32]; 11 tumor nodules from 8 mice were analyzed. In GEMM cohort, 13 endogenous tumor nodules were analyzed in seven 12- to 16-week-old *Ptft1a*$^{wt/cre}$*KRAS*$^{wt/G12D}$*p53*$^{fl/fl}$ (CKP) mice (GF = 5, non-GF = 8). Additional details are provided in the supplementary methods (Online Resource 1).

PET Imaging and Analysis

After 2 h of fasting, animals received [^{18}F]FDG intravenously (12 MBq/mouse, 20 MBq/rat). Dynamic PET/CT was performed in rats and GEMM for 90 min, whereas static imaging was performed in orthotopic mice (for 15 min) 120 min after tracer administration using a small-animal PET/CT scanner (Inveon, Siemens). PET-derived parameters included Standard uptake values $(SUV)_{mean}$, SUV_{max}, and mean tumor-to-muscle ratio (T/M_{mean}). Tumor regions were defined using corresponding histologic and T2-weighted MRI findings. Detailed acquisition, reconstruction, and image-analysis procedures are provided in the supplementary methods (Online Resource 1).

Clinical PET Imaging

The human study was approved by the ethics committee of the Faculty of Medicine, Technical University of Munich (protocol no. 181/17 S). In this retrospective study, 20 patients with PDAC who underwent [^{18}F]FDG PET/CT or PET/MRI in accordance with EANM guidelines were evaluated. Imaging was performed 86 ± 19 min after administration of 355.4 ± 90.2 MBq [^{18}F]FDG. Four tumors were excluded due to small size, extensive necrosis, or insufficient image quality (8m/8f; non-QM = 10/QM = 6). Additional details are provided in the supplementary methods (Online Resource 1; Supplemental table 1).

Histopathology and immunohistochemistry:

Murine tumors were histopathologically classified as C/QM or GF/non-GF [9] on H&E-stained sections and compared with the corresponding imaging findings. In patients, keratin 81 (KRT81) and Hepatocyte Nuclear Factor 1 Alpha (HNF1A) immunohistochemistry was performed on tissue microarrays of primary tumors, as previously described [6, 33], and classified according to the criteria in Supplemental Table 2. Detailed procedures are provided in the supplementary methods (Online Resource 1)

Statistical analysis

Statistical analyses were performed using GraphPad Prism 8.0.1. Normality was assessed using the Shapiro-Wilk test. Groups were compared using an unpaired two-tailed t-test for normally distributed data or the Mann-Whitney U test otherwise. $P < 0.05$ was considered statistically significant.

Results

Qualitative [^{18}F]FDG uptake patterns of PDAC subtypes across preclinical models and patients

C-HPAC cells exhibited epithelial and QM-PSN1 showed mesenchymal features i*n vitro* and in both heterotopic and orthotopic implanted xenografts (Fig. 1a). GEMM tumors showed high intertumoral heterogeneity and were classified as GF or non-GF (Fig. 1b) by their growth patterns[9]. Patient tumors

were classified as QM and non-QM based on KRT81 and HNF1A expression (Fig. 1c, Supplemental Table 2)[33].

[^{18}F]FDG uptake was visually higher in QM-PSN1 than in C-HPAC heterotopic and orthotopic xenografts (Fig. 2a). Likewise, non-GF tumors revealed higher uptake than GF tumors in GEMMs (Fig. 2b). Patients showed a similar visual trend, although the distinction between QM and non-QM tumors was less pronounced (Fig. 2c).

Distinct temporal [^{18}F]FDG uptake patterns in C/QM and GF/non-GF PDAC

QM-PSN1 cells exhibited sustained [^{18}F]FDG accumulation throughout the 90-min observation period, remaining consistently above C-HPAC cells (Fig. 3a). Similarly, heterotopic QM-PSN1 xenografts showed a continuous increase in T/M_{mean}, remaining higher than C-HPAC tumors, without overlap between groups (Fig. 3b). In GEMMs, [^{18}F]FDG uptake in non-GF tumors increased throughout the 90-min acquisition period, whereas most GF tumors reached a plateau by approximately 60 min (Fig. 3c). Across models, subtype-specific differences became more pronounced at later time points (Online Resource 1,. Supplementary Fig. 1), resulting in improved separation of morphologically heterogeneous tumors.

(a) *in vitro* [^{18}F]FDG uptake in 2-h-starved C-HPAC and QM-PSN1 cells, expressed as percentage uptake over 90 mins. **(b)** Dynamic [^{18}F]FDG uptake in fasted C-HPAC and QM-PSN1 subcutaneous rat venografts, and **(c)** in fasted GEMM GF/non-GF lesions.

[^{18}F]FDG PET revealed quantitative subtype-specific metabolic uptake differences across preclinical models and clinical cohort

QM-PSN1 cells showed 2.3 times higher [^{18}F]FDG uptake than C-HPAC cells *in vitro* (32.43 ± 6.70% vs. 13.98 ± 2.52%, $P < 0.0001$; Online Resource 1; Supplemental Fig. 1A). Similarly, QM-PSN1 tumors in heterotopic model revealed 2.6 times higher SUV_{max} than C-HPAC tumors with no overlap (6.91 ± 1.14 vs. 2.66 ± 0.28; $P < 0.0001$; Fig. 4a) and 2.0 times higher SUV_{max} in orthotopic models (2.85 ± 0.70 vs. 1.45 ± 0.50; $P = 0.0095$; Fig. 4a). In GEMMs, non-GF tumors showed 1.6 times higher SUV_{max} than GF tumors (3.94 ± 0.70 vs. 2.53 ± 0.97; $P = 0.0106$; Fig. 4b). In patients, QM tumors showed a similar but less pronounced trend with 1.3 times higher SUV_{max} compared to non-QM tumors (6.33 ± 1.74 vs. 4.95 ± 1.46; $P = 0.111$; Fig. 4c). Furthermore, QM patients had significantly shorter overall survival (12.11 ± 5.45 vs. 40.2 ± 29.26; $P = 0.0008$) than non-QM patients (Fig. 4d). Mechanistically, QM-PSN1 cells exhibited higher mRNA and protein levels of glucose transporter genes GLUT1 (SLC2A1) and GLUT3 (SLC2A3), and overexpressed Hexokinase 2 (HK2) (Online Resource1; Supplemental Fig. 2), an enzyme which catalyzes the first rate-limiting step of the glucolysis, which traps [^{18}F]FDG within the cell and is normally absent in healthy pancreatic tissue [34].

Comparative performance of [^{18}F]FDG PET-derived parameters for PDAC subtype stratification

Classification performance was evaluated using thresholds (described in the Supplemental Material) for SUV_{mean}, SUV_{max}, and T/M_{mean}. In heterotopic xenografts, all parameters achieved precision, sensitivity, specificity, and accuracy of 1.00 (Online Resource 1; Supplemental Table 3).

In orthotopic xenografts, GEMM, and patients, T/M_{mean} achieved the highest classification performance, whereas SUV_{mean} showed the lowest classification performance (Table 1; Fig. 4e).

Table 1

Diagnostic performance of [^{18}F]FDG PET parameters for differentiating PDAC subtypes. Calculated thresholds for SUV_{mean}, SUV_{max}, and T/M_{mean} were used to classify PDAC subtypes. Classification performance was assessed using precision, sensitivity, specificity, and accuracy.

Model	PET metrics	Threshold	Precision	Sensitivity	Specificity	Acurracy
Orthotopic(nude mice)	SUV_{mean}	1.5	0.83	1	0.83	0.91
Orthotopic (nude mice)	SUV_{max}	2.0	0.83	1	0.83	0.91
Orthotopic (nude mice)	T/M_{mean}	5.28	1	1	1	1
GEMM	SUV_{mean}	2.46	0.86	0.75	0.80	0.77
GEMM	SUV_{max}	3.32	0.86	0.75	0.80	0.77
GEMM	T/M_{mean}	9.47	0.89	1	0.89	0.92
Patients	SUV_{mean}	3.91	0.50	0.67	0.60	0.63
Patient	SUV_{max}	5.45	0.57	0.67	0.70	0.69
Patient	T/M_{mean}	5.8	0.63	0.83	0.70	0.75

Discussion

This study demonstrates that subtype-specific molecular and metabolic differences in PDAC can be detected non-invasively by [^{18}F]FDG PET. Across all preclinical models, QM/non-GF tumors consistently exhibited higher [^{18}F]FDG uptake than C/GF tumors, in line with the glycolytic phenotype previously associated with QM and the lipogenic profile of C/non-QM PDAC [29, 31]. PDAC subtypes with increased glycolysis and reduced cholesterol synthesis have been associated with greater tumor aggressiveness, poor survival, and diminished chemotherapy sensitivity compared with a more cholesterogenic

phenotype [4, 8, 27]. In our study, high [^{18}F]FDG accumulation observed in the QM PDAC cell line was associated with increased expression of genes involved in glucose transport (SLC2A1, SLC2A3) and phosphorylation (HK1, HK2). Notably, the more pronounced increase in HK2 than GLUT1 expression suggests that enhanced glucose phosphorylation and tracer retention, rather than transport alone, may primarily drive these differences. Our interpretation is supported by previous findings in hPDAC demonstrating a significant association between [^{18}F]FDG uptake and HK2, rather than GLUT1 expression[35]. Collectively, our results demonstrate that [^{18}F]FDG uptake reflects distinct molecular programs in PDAC and supports its use as a non-invasive biomarker for metabolic stratification of tumor aggressiveness.

Elevated [^{18}F]FDG PET-derived parameters, including SUV_{max}, MTV, and TLG have been associated with poor overall and disease-free survival in PDAC [15, 17, 36, 37] and several molecular studies have linked QM/non-GF and poorly differentiated PDAC to adverse outcomes [4, 8, 9, 27]. Increased [^{18}F]FDG accumulation has been reported in poorly differentiated tumors[28], however, its relationship with clinically relevant molecular subtypes remains unexplored. Using molecularly defined QM/C and GF/non-GF models across in vitro and in vivo systems, complemented by a retrospective patient cohort, we observed consistently higher [^{18}F]FDG uptake in the aggressive subtypes (QM/non-GF) particularly in preclinical models. QM tumors were also associated with shorter overall survival in patients. Our findings suggest that [^{18}F]FDG uptake captures biologically and clinically relevant subtype-specific metabolic differences and may serve as a non-invasive biomarker for PDAC stratification and prognostication.

Metabolic imaging is currently not part of the routine diagnostic or staging workup for PDAC. However, our findings strongly suggest that [^{18}F]FDG uptake may provide clinically relevant information beyond conventional anatomical imaging and warrant further evaluation for integration into diagnostic and treatment-planning pathways. The potential of metabolic imaging for molecular PDAC subtype discrimination is further supported by emerging MRI-based approaches. Hyperpolarized [1-^{13}C]pyruvate magnetic resonance spectroscopy has identified glycolytic PDAC tumors through increased pyruvate-to-lactate conversion [29], while deuterium metabolic imaging (DMI) has detected tumor-associated lactate production following administration of deuterated glucose in orthotopic PDAC models[38]. These techniques may complement [^{18}F]FDG PET by providing insights into downstream metabolic processes, although their value for non-invasive subtype discrimination in hPDAC remains to be established.

Beyond baseline tumor characterization, metabolic imaging may be particularly valuable for treatment monitoring. PDAC exhibits substantial metabolic plasticity, and therapy-induced metabolic adaptations can alter tumor vulnerabilities and phenotypic characteristics [39]. Such changes may be reflected by longitudinal alterations in [^{18}F]FDG uptake [21], raising the possibility that serial [^{18}F]FDG PET/CT could serve as a non-invasive biomarker of treatment response and subtype evolution. Future longitudinal studies integrating metabolic and volumetric response assessment are needed to determine whether

changes in [^{18}F]FDG uptake reflect treatment-induced metabolic reprogramming, subtype plasticity, or both.

Dynamic [18F]FDG PET revealed progressive divergence in uptake between PDAC phenotypes. Sustained tracer accumulation in QM/non-GF tumors, versus earlier plateauing in C/GF tumors, enhanced subtype discrimination at later imaging time points, especially using T/Mmean. These findings suggest that delayed imaging (≥ 90 min post-injection) may improve metabolic phenotyping, consistent with evidence that longer and standardized uptake periods increase tumor-to-background contrast, reproducibility, and quantitative accuracy of [^{18}F]FDG PET [40, 41]. While QM and C tumors were completely separated in homogeneous heterotopic and orthotopic xenografts, discrimination was reduced in GEMMs and patient cohorts, likely due to the heterogeneous microenvironment that affects tracer kinetics and retention [4, 29, 42, 43]. Similar overlap in [^{18}F]FDG PET SUV has been reported in hPDAC stratified by tumor grade [28]. T/M_{mean} consistently showed the best classification performance across all models. This supports the use of reference tissue normalization as a means of reducing biological and technical variability beyond absolute SUV measurements, consistent with previous studies of pancreatic lesions [44]. Together, our findings suggest that longer uptake times and use of muscle as reference tissue may improve subtype discrimination in PDAC patients by increasing the contribution of tumor-specific tracer trapping relative to background uptake.

Several limitations of our study warrant consideration. The small preclinical and retrospective surgical patient cohort limits generalizability and likely underrepresents aggressive QM/non-GF tumors, which are less often resected due to advanced disease[45]. In addition, PET quantification may be affected by scanner- and acquisition-related variability, tumor heterogeneity, partial volume effects, and necrosis[46, 47]. Transcriptomic and proteomic analyses were restricted to two PDAC cell lines and were not validated in the corresponding tumors due to the absence of spared samples. Finally, patient subtypes were defined using surrogate immunohistochemical markers (KRT81, HNF1A) rather than comprehensive molecular profiling [4], and the proposed classification thresholds were not independently validated, requiring confirmation in larger prospective cohorts. Therefore, larger prospective studies incorporating standardized imaging protocols, longitudinal imaging, and molecular profiling are needed to establish and validate robust classification thresholds.

Conclusion

[^{18}F]FDG uptake differs across PDAC subtypes, with higher tracer accumulation in QM/non-GF than C/GF tumors across preclinical models and a similar trend in patients. Delayed imaging (≥ 90 min post-injection) and reference-tissue normalization improved subtype discrimination, highlighting the potential of [^{18}F]FDG PET for non-invasive metabolic phenotyping. Larger prospective studies with longitudinal imaging and molecular validation are needed to confirm these findings and define robust classification thresholds.

Declarations

Financial support:

This work was supported by funding from the German Federal Ministry of Education and Research (grant 13N16450 QuE-MRT) to F.S., R.B., and I.H., Wilhelm Sander Foundation (grant 2023.083.1) to R.B. and I.H., and German Research Foundation (DFG) within the Collaborative Research Center-Initiative 824 (project C6, and Z2R to R.B. and F.S.)

Acknowledgements

We thank Geoffrey Topping, Irina Skuratovska, Sybille Reder, and Michael Baggio Lorenz for their excellent experimental and technical support.

Funding:

This work was supported by funding from the German Federal Ministry of Education and Research (grant 13N16450 QuE-MRT) to F.S., R.B., and I.H., Wilhelm Sander Foundation (grant 2023.083.1) to R.B. and I.H., and German Research Foundation (DFG) within the Collaborative Research Center-Initiative 824 (project C6, and Z2R to R. B. and F.S.).

Competing Interests

The authors have no relevant financial or non-financial interests to disclose.

Author Contributions

Conception and design: R.K., R.B., and I.H. Development of methodology: R.K., M.M., H.T., F.S., K.S., R.B., L.S., and I.H. Acquisition of data: R.K., M.M., L.K, M.Mh., A.M., H.T., K.S., L.S., and I.H. Analysis and interpretation of data: R.K., M.M., A.M., L.S., and I.H. Writing and/or revision of the manuscript: R.K., L.S., R.B., and I.H. Administrative, technical, or material support: S.K., K.S., F.S., R.B., and I.H. Study supervision: R.B., and I.H. All authors reviewed and approved the final manuscript.

Data Availability

The datasets generated and/or analyzed during the current study are available from the

corresponding author on reasonable request.

Ethics approval

All animal experiments were performed in compliance with the European guidelines for the care and use of laboratory animals. The animal study was approved by Regierung von Oberbayern, Munich, Germany (license 55.2-2532.Vet_02-18-91).

The human study was approved by the Ethics Committee of the Faculty of Medicine, Technical University of Munich (protocol no. 181 17 S). Clinical trial number: not applicable.

Consent to participate and publish

Informed consent was waived for all individual participants included in the study.

References

1. Siegel RL, Kratzer TB, Giaquinto AN, Sung H, Jemal A (2025) Cancer statistics, 2025. CA Cancer J Clin 75:10–45. https://doi.org/10.3322/caac.21871
2. Danpanichkul P, Pang Y, Tothanarungroj P, Dejvajara D, Kim D, Saokhieo P et al (2026) Gastrointestinal cancer statistics in 2022 and projection to 2050: GLOBOCAN estimates across 185 countries. Cancer 132:e70245. https://doi.org/10.1002/cncr.70245
3. Evan T, Wang VM-Y, Behrens A (2022) The roles of intratumour heterogeneity in the biology and treatment of pancreatic ductal adenocarcinoma. Oncogene 41:4686–4695. https://doi.org/10.1038/s41388-022-02448-x
4. Collisson EA, Bailey P, Chang DK, Biankin AV (2019) Molecular subtypes of pancreatic cancer. Nat Rev Gastroenterol Hepatol 16:207–220. https://doi.org/10.1038/s41575-019-0109-y
5. Collisson EA, Sadanandam A, Olson P, Gibb WJ, Truitt M, Gu S et al (2011) Subtypes of pancreatic ductal adenocarcinoma and their differing responses to therapy. Nat Med 17:500–503. https://doi.org/10.1038/nm.2344
6. Muckenhuber A, Berger AK, Schlitter AM, Steiger K, Konukiewitz B, Trumpp A et al (2018) Pancreatic Ductal Adenocarcinoma Subtyping Using the Biomarkers Hepatocyte Nuclear Factor-1A and Cytokeratin-81 Correlates with Outcome and Treatment Response. Clin Cancer Res 24:351–359. https://doi.org/10.1158/1078-0432.CCR-17-2180
7. Bailey P, Chang DK, Nones K, Johns AL, Patch A-M, Gingras M-C et al (2016) Genomic analyses identify molecular subtypes of pancreatic cancer. Nature 531:47–52. https://doi.org/10.1038/nature16965
8. Aung KL, Fischer SE, Denroche RE, Jang G-H, Dodd A, Creighton S et al (2018) Genomics-Driven Precision Medicine for Advanced Pancreatic Cancer: Early Results from the COMPASS Trial. Clin Cancer Res 24:1344–1354. https://doi.org/10.1158/1078-0432.CCR-17-2994
9. Kalimuthu N, Wilson S, Grant GW, Seto RC, O'Kane M, Vajpeyi G (2020) Morphological classification of pancreatic ductal adenocarcinoma that predicts molecular subtypes and correlates with clinical outcome. Gut 69:317–328. https://doi.org/10.1136/gutjnl-2019-318217
10. O'Kane GM, Grünwald BT, Jang G-H, Masoomian M, Picardo S, Grant RC et al (2020) GATA6 Expression Distinguishes Classical and Basal-like Subtypes in Advanced Pancreatic Cancer. Clin Cancer Res 26:4901–4910. https://doi.org/10.1158/1078-0432.CCR-19-3724

11. Lansbergen MF, Dings MPG, Manoukian P, Fariña A, Waasdorp C, Hooijer GKJ et al (2024) Transcriptome-based classification to predict FOLFIRINOX response in a real-world metastatic pancreatic cancer cohort. Transl Res 273:137–147. https://doi.org/10.1016/j.trsl.2024.08.002
12. Robertson FP, Cameron A, Spiers HVM, Joseph N, Taylor E, Ratnayake B et al (2024) Evidence for molecular subtyping in pancreatic ductal adenocarcinoma: a systematic review. HPB 26:609–617. https://doi.org/10.1016/j.hpb.2024.02.001
13. Kaissis GA, Ziegelmayer S, Lohöfer FK, Harder FN, Jungmann F, Sasse D et al (2020) Image-Based Molecular Phenotyping of Pancreatic Ductal Adenocarcinoma. J Clin Med 9:724. https://doi.org/10.3390/jcm9030724
14. Kaissis G, Ziegelmayer S, Lohöfer F, Steiger K, Algül H, Muckenhuber A et al (2019) A machine learning algorithm predicts molecular subtypes in pancreatic ductal adenocarcinoma with differential response to gemcitabine-based versus FOLFIRINOX chemotherapy. Real FX, editor. PLoS ONE 14:e0218642. https://doi.org/10.1371/journal.pone.0218642
15. Albano D, Familiari D, Gentile R, Scalisi S, Midiri F, Messina M et al (2018) Clinical and prognostic value of 18F-FDG-PET/CT in restaging of pancreatic cancer. Nucl Med Commun 39:741–746. https://doi.org/10.1097/MNM.0000000000000862
16. Pauwels EKJ, Coumou AW, Kostkiewicz M, Kairemo K (2013) [^{18}F]Fluoro-2-Deoxy-D-Glucose Positron Emission Tomography/Computed Tomography Imaging in Oncology: Initial Staging and Evaluation of Cancer Therapy. Med Princ Pract 22:427–437. https://doi.org/10.1159/000346303
17. Wang Z, Chen J-Q, Liu J-L, Qin X-G, Huang Y (2013) FDG-PET in diagnosis, staging and prognosis of pancreatic carcinoma: a meta-analysis. World J Gastroenterol 19:4808–4817. https://doi.org/10.3748/wjg.v19.i29.4808
18. Kim Y, Cheon GJ, Kang SY, Paeng JC, Kang KW, Lee DS et al (2018) Prognostic value of simultaneous 18F-FDG PET/MRI using a combination of metabolo-volumetric parameters and apparent diffusion coefficient in treated head and neck cancer. EJNMMI Res 8:2. https://doi.org/10.1186/s13550-018-0357-9
19. Lee JW, Kang CM, Choi HJ, Lee WJ, Song SY, Lee J-H et al (2014) Prognostic Value of Metabolic Tumor Volume and Total Lesion Glycolysis on Preoperative^{18} F-FDG PET/CT in Patients with Pancreatic Cancer. J Nucl Med 55:898–904. https://doi.org/10.2967/jnumed.113.131847
20. Riviere D, Aarntzen E, Van Geenen E, Chang D, De Geus-Oei L-F, Brosens L et al (2024) Qualitative flow metabolic phenotype of pancreatic cancer. A new prognostic biomarker? HPB. 26:389–399. https://doi.org/10.1016/j.hpb.2023.11.010
21. Harder FN, Jungmann F, Kaissis GA, Lohöfer FK, Ziegelmayer S, Havel D et al (2021) [18F]FDG PET/MRI enables early chemotherapy response prediction in pancreatic ductal adenocarcinoma. EJNMMI Res 11:70. https://doi.org/10.1186/s13550-021-00808-4
22. Luo J (2021) KRAS mutation in pancreatic cancer. Semin Oncol 48:10–18. https://doi.org/10.1053/j.seminoncol.2021.02.003

23. Ying H, Kimmelman AC, Lyssiotis CA, Hua S, Chu GC, Fletcher-Sananikone E et al (2012) Oncogenic Kras Maintains Pancreatic Tumors through Regulation of Anabolic Glucose Metabolism. Cell 149:656–670. https://doi.org/10.1016/j.cell.2012.01.058
24. Yun J, Rago C, Cheong I, Pagliarini R, Angenendt P, Rajagopalan H et al (2009) Glucose Deprivation Contributes to the Development of *KRAS* Pathway Mutations in Tumor Cells. Science 325:1555–1559. https://doi.org/10.1126/science.1174229
25. Varghese AM, Perry MA, Chou JF, Nandakumar S, Muldoon D, Erakky A et al (2025) Clinicogenomic landscape of pancreatic adenocarcinoma identifies KRAS mutant dosage as prognostic of overall survival. Nat Med 31:466–477. https://doi.org/10.1038/s41591-024-03362-3
26. Mueller S, Engleitner T, Maresch R, Zukowska M, Lange S, Kaltenbacher T et al (2018) Evolutionary routes and KRAS dosage define pancreatic cancer phenotypes. Nature 554:62–68. https://doi.org/10.1038/nature25459
27. Karasinska JM, Topham JT, Kalloger SE, Jang GH, Denroche RE, Culibrk L et al (2020) Altered Gene Expression along the Glycolysis–Cholesterol Synthesis Axis Is Associated with Outcome in Pancreatic Cancer. Clin Cancer Res 26:135–146. https://doi.org/10.1158/1078-0432.CCR-19-1543
28. Ahn SJ, Park M-S, Lee JD, Kang WJ (2014) Correlation between 18F-fluorodeoxyglucose positron emission tomography and pathologic differentiation in pancreatic cancer. Ann Nucl Med 28:430–435. https://doi.org/10.1007/s12149-014-0833-x
29. Heid I, Münch C, Karakaya S, Lueong SS, Winkelkotte AM, Liffers ST et al (2022) Functional noninvasive detection of glycolytic pancreatic ductal adenocarcinoma. Cancer Metab 10:24. https://doi.org/10.1186/s40170-022-00298-5
30. Topping GJ, Heid I, Trajkovic-Arsic M, Kritzner L, Grashei M, Hundshammer C et al (2021) Hyperpolarized 13C Spectroscopy with Simple Slice-and-Frequency-Selective Excitation. Biomedicines 9:121. https://doi.org/10.3390/biomedicines9020121
31. Daemen A, Peterson D, Sahu N, McCord R, Du X, Liu B et al (2015) Metabolite profiling stratifies pancreatic ductal adenocarcinomas into subtypes with distinct sensitivities to metabolic inhibitors. Proc Natl Acad Sci [Internet]. [cited 2025 Jan 8];112 https://doi.org/10.1073/pnas.1501605112
32. Karampour R, Steinhelfer L, Liu J, Balaji A, Weidle S, Steiger K et al (2026) Hemorrhage-Induced Bias of [18F]FDG PET Signal Interpretation in Pancreatic Ductal Adenocarcinoma [Internet]. [cited 2026 Oct 26] https://doi.org/10.21203/rs.3.rs-10932499/v1
33. Rao J, Sinn M, Pelzer U, Riess H, Oettle H, Demir IE et al (2024) KRT81 and HNF1A expression in pancreatic ductal adenocarcinoma: investigation of predictive and prognostic value of immunohistochemistry-based subtyping. J Pathol Clin Res 10:e12377. https://doi.org/10.1002/2056-4538.12377
34. Salas JR, Clark PM (2022) Signaling Pathways That Drive^{18} F-FDG Accumulation in Cancer. J Nucl Med 63:659–663. https://doi.org/10.2967/jnumed.121.262609
35. Higashi T, Saga T, Nakamoto Y, Ishimori T, Mamede MH, Wada M et al (2002) Relationship between retention index in dual-phase (18)F-FDG PET, and hexokinase-II and glucose transporter-1

expression in pancreatic cancer. J Nucl Med Off Publ Soc Nucl Med 43:173–180

36. Zhu D, Wang L, Zhang H, Chen J, Wang Y, Byanju S et al (2017) Prognostic value of 18F-FDG-PET/CT parameters in patients with pancreatic carcinoma: A systematic review and meta-analysis. Med (Baltim) 96:e7813. https://doi.org/10.1097/MD.0000000000007813
37. Hwang JP, Lim I, Chang KJ, Kim BI, Choi CW, Lim SM (2012) Prognostic value of SUVmax measured by Fluorine-18 Fluorodeoxyglucose Positron Emission Tomography with Computed Tomography in Patients with Pancreatic Cancer. Nucl Med Mol Imaging 46:207–214. https://doi.org/10.1007/s13139-012-0151-y
38. Markovic S, Roussel T, Agemy L, Sasson K, Preise D, Scherz A et al (2021) Deuterium MRSI characterizations of glucose metabolism in orthotopic pancreatic cancer mouse models. NMR Biomed 34:e4569. https://doi.org/10.1002/nbm.4569
39. Peschke K, Jakubowsky H, Schäfer A, Maurer C, Lange S, Orben F et al (2022) Identification of treatment-induced vulnerabilities in pancreatic cancer patients using functional model systems. EMBO Mol Med 14:e14876. https://doi.org/10.15252/emmm.202114876
40. Houshmand S, Salavati A, Basu S, Khiewvan B, Alavi A (2014) The role of dual and multiple time point imaging of FDG uptake in both normal and disease states. Clin Transl Imaging 2:281–293. https://doi.org/10.1007/s40336-014-0075-x
41. Hesketh RL, Lewis DY, Brindle KM (2024) Optimisation of Animal Handing and Timing of 2-deoxy-2-[18F]fluoro-D-glucose PET Tumour Imaging in Mice. Mol Imaging Biol 26:965–976. https://doi.org/10.1007/s11307-024-01956-4
42. Heid I, Steiger K, Trajkovic-Arsic M, Settles M, Eßwein MR, Erkan M et al (2017) Co-clinical Assessment of Tumor Cellularity in Pancreatic Cancer. Clin Cancer Res 23:1461–1470. https://doi.org/10.1158/1078-0432.CCR-15-2432
43. Murakami K (2011) FDG-PET for hepatobiliary and pancreatic cancer: Advances and current limitations. World J Clin Oncol 2:229. https://doi.org/10.5306/wjco.v2.i5.229
44. Utsunomiya T, Ogawa K, Funamizu N, Sakamoto K, Watanabe J, Otani H et al (2022) The tumor-to-liver ratio of the standardized uptake value is a useful FDG-PET/CT parameter for predicting malignant intraductal papillary mucinous neoplasm of the pancreas. Ann Gastroenterol Surg 6:695–703. https://doi.org/10.1002/ags3.12562
45. Kimura W, Morikane K, Esaki Y, Chan WC, Pour PM (1998) Histologic and biologic patterns of microscopic pancreatic ductal adenocarcinomas detected incidentally at autopsy. Cancer 82(19980515):1839–1849. https://doi.org/10.1002/(SICI)1097-0142.)82:10%3C1839::AID-CNCR5%3E3.0.CO;2-I
46. Hoetjes NJ, Van Velden FHP, Hoekstra OS, Hoekstra CJ, Krak NC, Lammertsma AA et al (2010) Partial volume correction strategies for quantitative FDG PET in oncology. Eur J Nucl Med Mol Imaging 37:1679–1687. https://doi.org/10.1007/s00259-010-1472-7
47. Boellaard R, Herrmann K, Barrington SF, Cranston I, Mottaghy FM, Hoekstra CJ et al (2025) [18F]FDG PET/CT: EANM procedure guidelines for tumour imaging: version 3.0. EANM J 1:100006.

https://doi.org/10.1016/j.eanmj.2025.100006

Figures

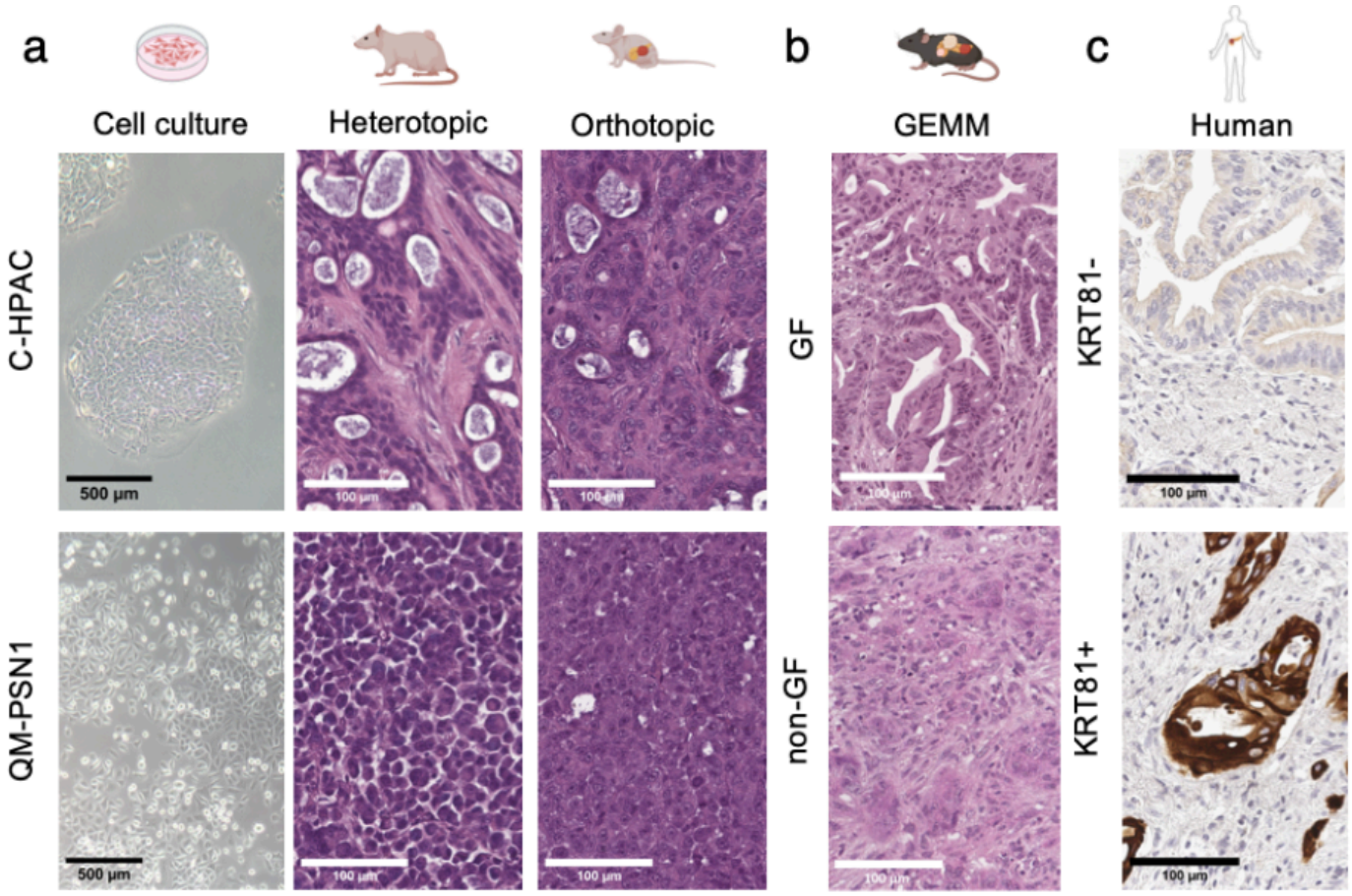


Figure 1

Morphological differences between C/QM and GF/non-GF PDAC subtypes *in vitro*, *in vivo,* and in patients. Representative photomicrographs of **(a)** C-HPAC and QM-PSN1 in cell culture (10x), rodent xenografts (40x), and **(b)** GF and non-GF tumors in GEMM as indicated (40x). **(c)** Representative KRT81 staining of QM and non-QM tumors in patients (40x).

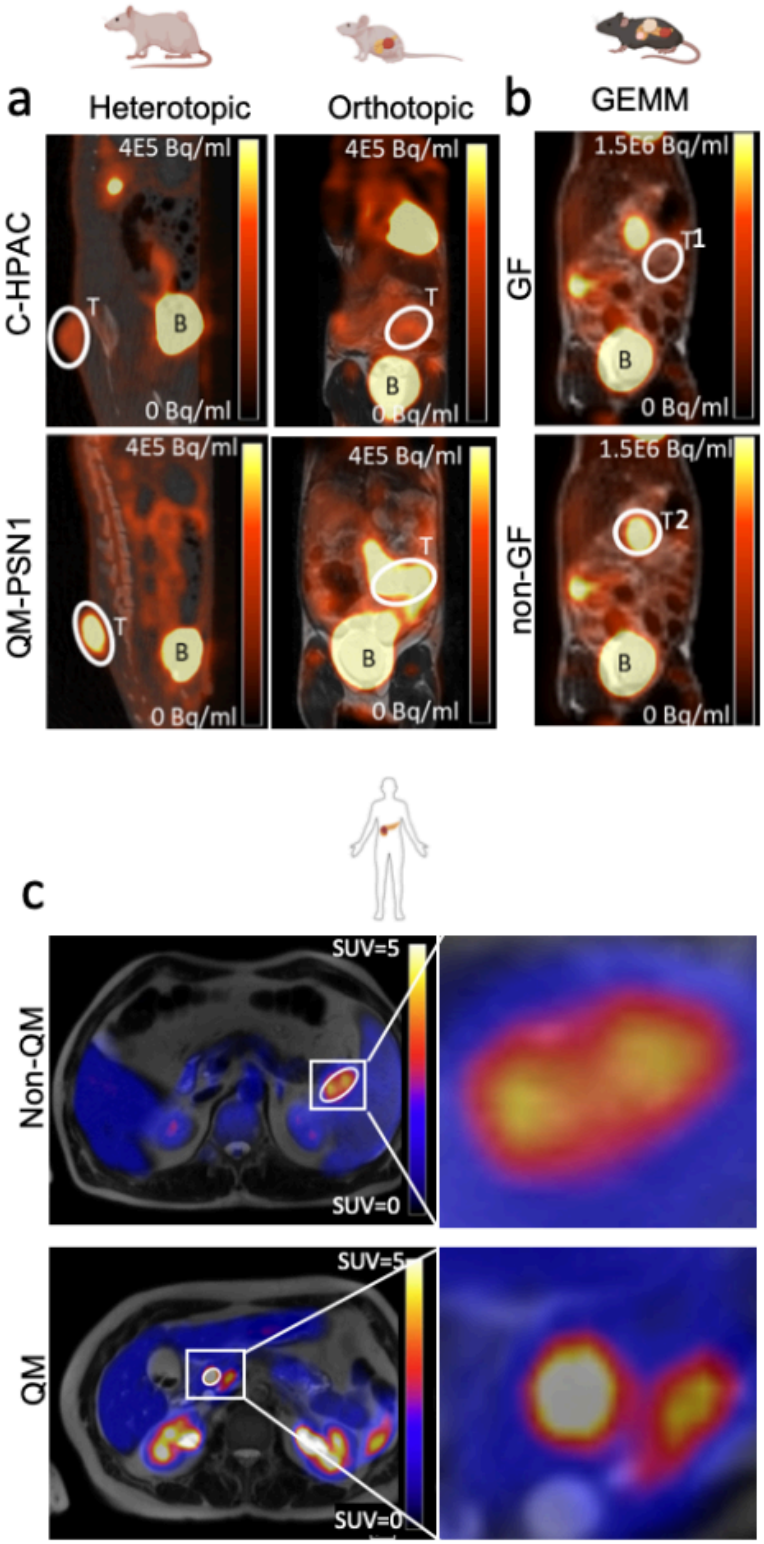


Figure 2

Subtype-specific qualitative [^{18}F]FDG PET uptake across preclinical models and patients.

Representative [^{18}F]FDG PET images of **(a)** sagittal heterotopic and coronal orthotopic C-HPAC and QM-PSN1 tumors, **(b)** GF (T1) and non-GF(T2) tumors within the same GEMM animal, and **(c)** KRT81- (non-QM) and KRT81+ (QM) tumors in PDAC patients.

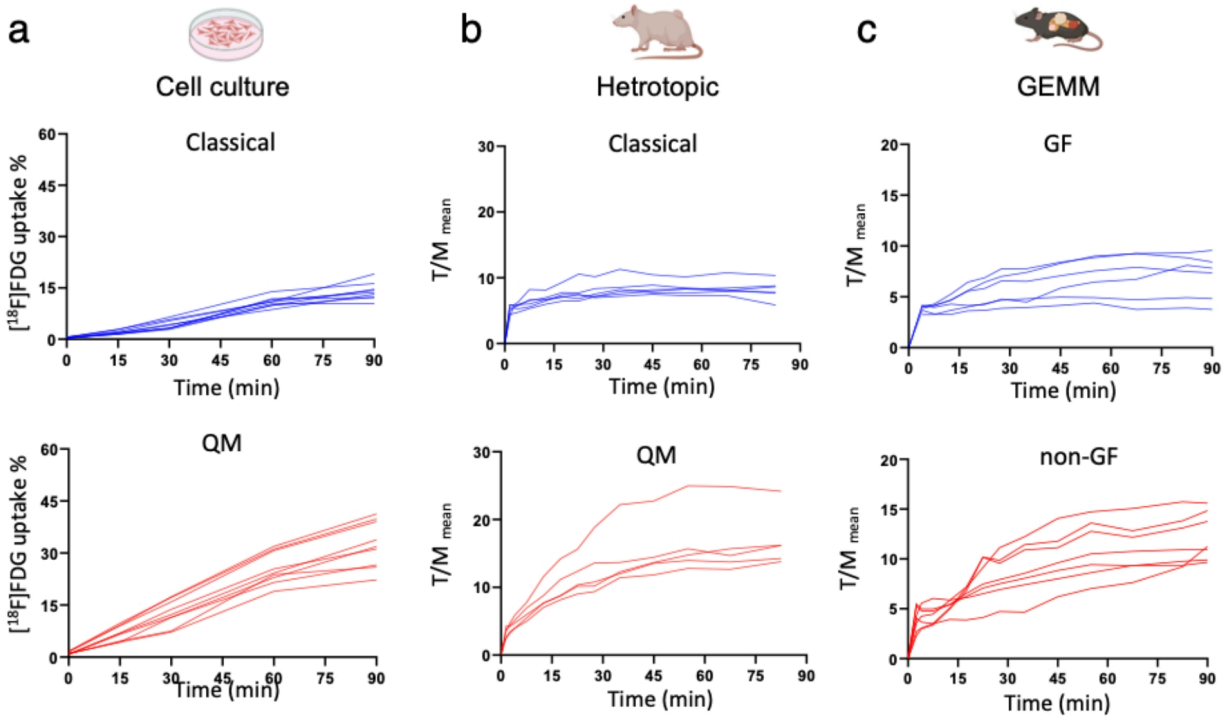


Figure 3

Dynamic [^{18}F]FDG uptake kinetics of PDAC subtypes across preclinical models.

(a) *in vitro* [^{18}F]FDG uptake in 2-h-starved C-HPAC and QM-PSN1 cells, expressed as percentage uptake over 90 mins. **(b)** Dynamic [^{18}F]FDG uptake in fasted C-HPAC and QM-PSN1 subcutaneous rat venografts, and **(c)** in fasted GEMM GF/non-GF lesions.

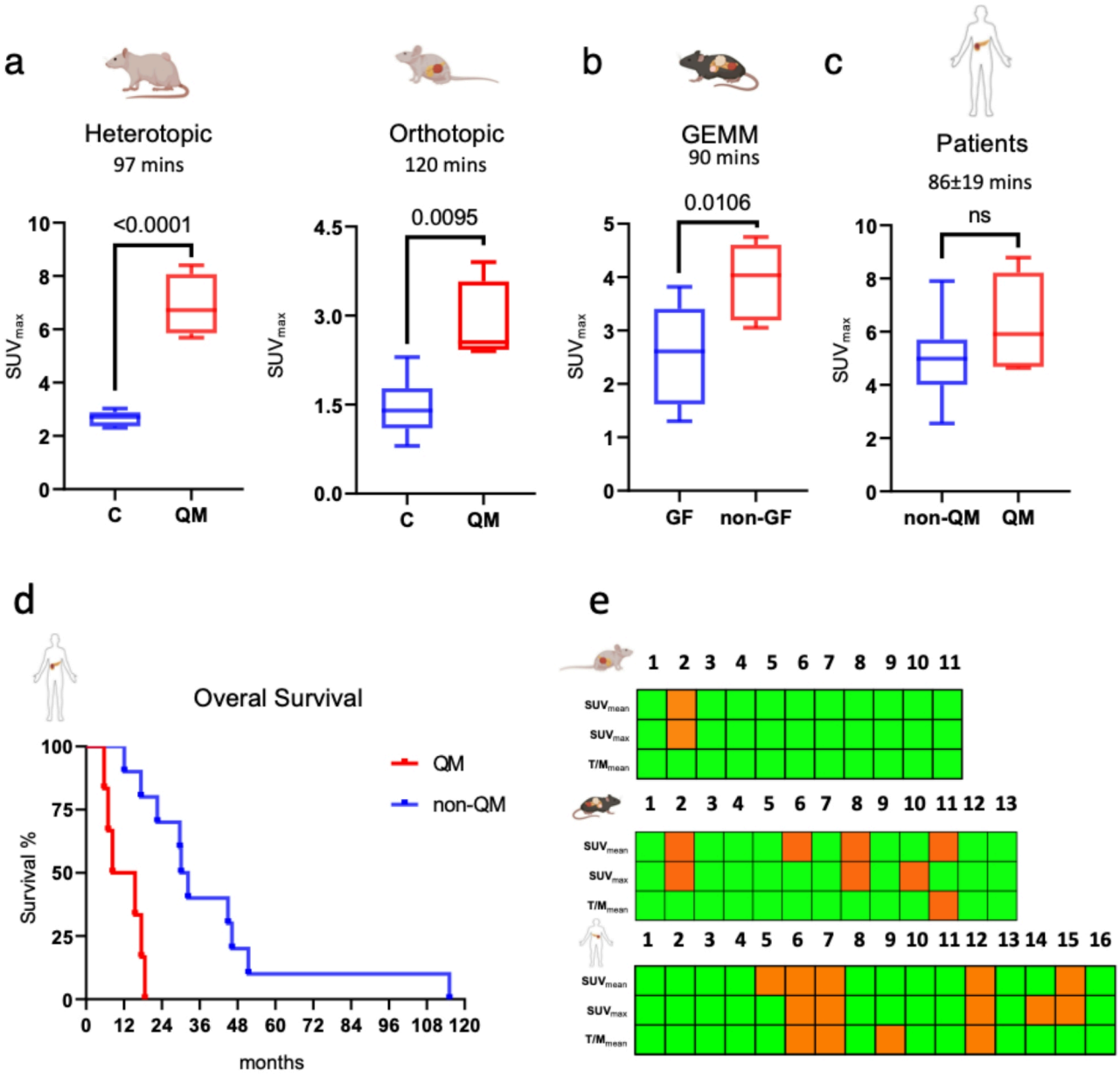


Figure 4

Quantitative [^{18}F]FDG PET-derived parameters differentiate PDAC phenotypes across preclinical models and patients. Box-and-whisker plots show [^{18}F]FDG uptake in C/QM and GF/non-GF phenotypes across **(a)** implanted models, **(b)** GEMMs, and (**c**) patients. **(d)** Kaplan–Meier survival curves comparing overall survival (OS) between PDAC patients with QM and non-QM subtypes (log-rank test). **(e)** Heatmaps of classification outcomes for individual tumors (green = correct; orange = misclassified) for SUV_{mean}, SUV_{max}, and T/M_{mean}.

Supplementary Files

This is a list of supplementary files associated with this preprint. Click to download.

- 09.11.2026SupplementalUnlinked2.docx